Available online at www.sciencedirect.com

ScienceDirect

Procedia CIRP 124 (2024) 16–19

www.elsevier.com/locate/procedia

13th CIRP Conference on Photonic Technologies [LANE 2024], 15-19 September 2024, Fürth, Germany

Dissimilar laser welding of high-thickness Cu/Al plates for high-current density electrical batteries

Michele Francioso[a,*], Erica Liverani[a], Alessandro Ascari[a], Alessandro Fortunato[a]

[a]*University of Bologna, Viale Risorgimento 2, Bologna, 40136, Italy*

* Corresponding author. *E-mail address:* michele.francioso2@unibo.it

Abstract

Electrical batteries connecting is a crucial phase in the fabrication of electrical vehicles. It is usually performed using high-quality lasers focused on narrow spot, to overcome the low optical absorptivity of copper and/or aluminum and displaced with high-speed scanner to accomplish the production rate. In applications where the current density is high (naval, heavy transport, etc) the busbars used for the electrical connections are thick (0.8-1 mm) increasing the difficulties of having joints with no defects. In this paper, an in-depth analysis of the impact of laser power, welding speed, and innovative scanning strategy on joint quality is presented for lap welding of nickel-plated copper (0.8 mm) to AA1050 alloy (3 mm). Process optimization involves achieving the desired weld area while controlling metal-mixing indices to limit the formation of brittle intermetallic compounds, cracks and voids. Weld joint quality assessment, including metallographic examination, microhardness tests and SEM-EDX analysis is presented and discussed.

Keywords: Laser Welding; Dissimilar Materials; Lithium-ion betteries; e-mobility;

1. Introduction

EU established CO_2 emission standards in 2019 for heavy-duty vehicles with reduction targets of 15% by 2025 and 30% by 2030 compared to the reference period of July 2019 to June 2020. Electrifying heavy-duty vehicles is crucial for meeting these goals, and developing high-performance electric drivetrain systems is a key step in this process. Laser beam welding (LBW) is widely used in the automotive sector, particularly in battery production for electric vehicles. Production of batteries for heavy electric vehicles to handle high current densities is essential to ensure the safety, durability and reliability of these vehicles in their lifecycle. In this context, LBW offers controlled energy input and precision during the process [1]. Copper (Cu) and aluminum (Al) are the most used materials for cell-to-busbar joints in battery production due to their physical properties, offering good mechanical performance and high electrical conductance. Depending on cell architecture, Cu and Al plates for heavy-duty applications can have a thickness of around one millimeter. The formation of brittle intermetallic compounds (IMCs), low absorption of laser radiation, and differences in material properties possess huge challenges for the lap joints of thicker plates [2]. Intermetallic compounds play a crucial role in determining the mechanical [3] and electrical [4] performance of Cu-Al welded joints. IMCs formed by copper and aluminum have lower ductility than the base materials, which favors the initiation of cracks in these regions. The presence of IMCs leads to changes of grain size and dislocation density within the diffusion zone, limiting the flow of electrical current across the interface and increases the overall resistivity [5]. A previous study [6] used a spiral strategy for low thicknesses welding, ranging from 0.2 mm to 0.4 mm. This revealed that maintaining an appropriate spiral separation distance (SD) effectively prevented the overlapping of adjacent welds and ensured sufficient heat input. However, this study

10.1016/j.procir.2024.08.062

focuses on using this strategy with larger thickness. This research aims to study the influence of power, energy density, and laser scanning paths on Cu/Al lap joint welding characteristics. The welding process parameters are observed and compared to examine various welding aspects. To detect intermetallic compounds (IMCs) within the joints, SEM-EDS analysis and micro-indentations for hardness are used. Additionally, an image-based clustering algorithm is applied to quantify defects like porosity and IMCs in the weld bead while correlating them with the process parameters.

2. Materials and Methods

2.1. Laser welding setup

A Yb:Fiber CW multi-mode laser power source was used in the welding configuration as shown in Table 1. The laser beam was focused and moved using a galvo scanner.

Table 1. Welding equipment

Properties	UoM	Value
Laser Source		nLight Alta 2.5 kW
Scanner head		Scanlab HurryScan 30
Control board		Scanlab RTC5
Focal length	[mm]	163
Collimation distance	[mm]	120
Fiber diameter	[µm]	50
BPP	[mm· mrad]	2
Spot diameter	[µm]	65

The investigation was carried out utilizing a lap-welding, with a 0.8 mm thick nickel-coated copper plate (C11000) on top of a 3 mm thick aluminum plate (AA 1050).

Before welding, the plates were thoroughly cleaned to remove any contamination and then clamped to eliminate any gaps. No shielding gas was used during the welding process, and to protect the scanning optics, a high-pressure lateral air jet was employed. The laser beam was focused onto the copper plate surface without any tilting action. Fig. 1 illustrates the welding configuration, including the scanning approach that uses an Archimedean spiral pattern starting from the center to the outer periphery, with a maximum radius of 1.5 mm. The spacing between each spiral, known as the separation distance, was adjusted from 0.2 mm to 0.6 mm to examine various welding paths.

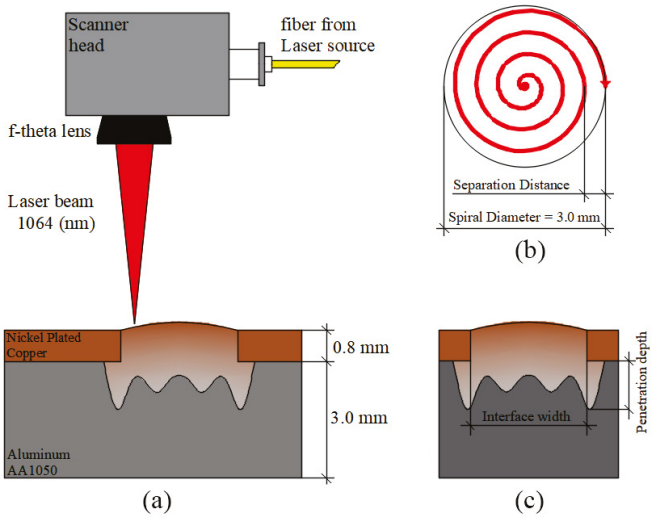

Fig. 1. (a) Laser Welding configuration, (b) Welding path details, (c) weld seam characteristics.

Table 2. Process parameters

Factors	UoM	Levels
Laser power	[W]	1200; 1500; 1800
Welding speed	[mm/s]	150; 200
Separation distance	[mm]	0.2; 0.4; 0.6

This study developed a mixed-level factorial design incorporating varying levels of laser power, welding speed, and separation distance within the spiral pattern, shown in Table 2. Each trial was repeated three times.

2.2. Weld Beads characterization

In order to evaluate the morphological characteristics and potential defects of the weld beads, the specimens were cut by a Wire EDM machine, then embedded in resin, and polished.

The metallographic samples were etched using a 50% nitric acid (HNO_3) solution and 50% distilled water.

The weld seams were examined through micrographs before and after the chemical etching, utilizing a Keyence VHX700 optical microscope (OM). The regions of the weld beads identified with different copper/aluminum mixing were then analyzed using SEM-FEG microscopy (Tescan Mira3 with a Schottky emitter) with an EDS system (Bruker X-Flash 630M) for micro elemental analysis. Finally, Vickers microhardness tests were conducted in the aforementioned key regions, using a durometer (HX-1000, Remet) with 0.2 kg load (HV0.2) and a dwell time of 10 s.

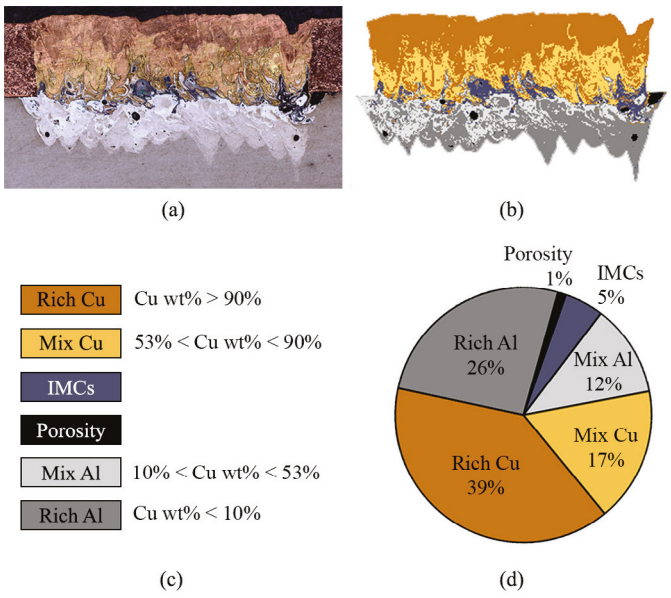

Fig. 2. Steps of the image analysis: a) OM picture, b) digitalisation of the OM, c) clustering of main regions and d) areas calculation.

2.3. Image analysis algorithm

An algorithm for image analysis was developed in MATLAB using microstructural characterization to identify specific welding regions, with a focus on areas emerging across intermetallic compounds and porosity. Reference samples were used to correlate each region with a specific chromatic feature range with color thresholding and established a link between the chemical properties and visual attributes. This algorithm accurately measured the area of each identified zone, thereby offering precise details regarding the distribution and size of these regions within the weld bead. The pores have been determined using the same technique, using black color, and a circularity criterion was also used for smaller pores to identify these defects accurately. To assess the efficiency of the proposed approach, a comparison was made between the findings from SEM-EDS analysis and those suggested by the clustering algorithm in the validation sample. Fig. 2 shows the main steps of the described method.

3. Results

3.1. Weld geometry

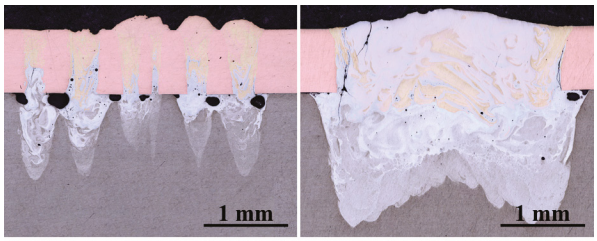

(a) (b)

Fig. 3. Weld beads with fragmented (a) and fully unified interface (b)

The OMs of each sample were acquired for weld geometry evaluation. Upon initial examination, it was observed that the weld bead exhibited incomplete fusion or minimal penetration at a power of 1200 W, hence these samples were excluded from subsequent analysis.

Table 3. Weld results.

Laser power [W]	Welding speed [mm/s]	Separation Distance [mm]	Energy density [10^6J/cm^2]	Penetration Depth [mm]	Interface Width [mm]
1500	150	0.6	3.6	0.47	0.50
1500	200	0.6	2.7	0.12	0.29
1500	150	0.4	5.4	0.66	0.94
1500	200	0.4	4.0	0.22	0.30
1500	150	0.2	10.7	0.95	2.68
1500	200	0.2	8.1	0.68	1.97
1800	150	0.6	4.4	1.12	1.22
1800	200	0.6	3.3	0.78	0.65
1800	150	0.4	6.5	1.34	1.57
1800	200	0.4	4.9	0.92	1.54
1800	150	0.2	12.9	1.64	2.81
1800	200	0.2	9.7	1.19	2.92

However, at 1500 W and 1800 W, two forms of weld penetrations were distinguished based on interface appearances, as shown in Fig. 3. Fragmented interfaces were frequently present in tests conducted with greater separation distance, and fully unified interface, typically found in tests conducted with smaller separation distances.

To characterize the weld bead from an energetic perspective, the energy density of the weld bead was calculated as the product of irradiance and interaction time.

Each test's average penetration depth and interface values are presented in Table 3.

3.2. Microstructure characterization

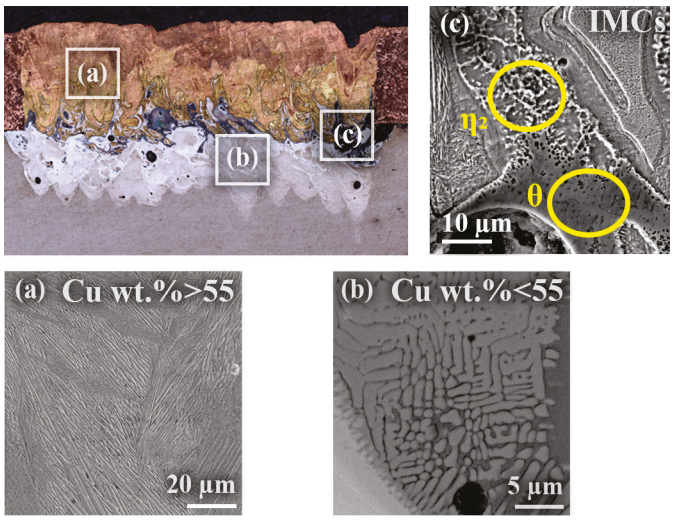

Fig. 4. FEG-SEM EDS maps of classified areas: (a) Copper-rich; (b) Aluminium-rich; (c) IMCs.

Samples were analyzed with FEG-SEM EDS maps and spectrums were evaluated to identify the distribution of the alloy elements. Six regions were initially identified, but from a process optimization point of view, four final areas have been classified (Fig. 4): i) copper-rich, ii) aluminum-rich, iii) IMCs region, and iv) pores. Considering the IMCs area, the measured chemical compositions were in-line with the composition of phases θ ($CuAl_2$) and η_2 (CuAl). Table 4 shows the chemical composition of the IMCs found in weld beads. Most of the samples showed θ in the interface area and η_2 phase close to external cracks (where present).

Table 4. IMCs Chemical composition wt.% and hardness measurements.

IMCs phase	Cu [wt.%]	Al [wt.%]	HV mean	HV Std.Dev.
θ ($CuAl_2$)	53.6	46.4	569	112
η_2 (CuAl)	70.4	29.6	739	161

Micro-indentations were conducted to assess the hardness in the regions previously identified as IMCs. Table 4 presents the mean hardness values from these areas. The obtained values confirm the identified phases [7]. Due to the brittle nature of both identified IMCs, the image algorithm considers both phases collectively as potentially critical areas.

3.3. Clustering image analysis

Following the previous results, the clustering algorithm was used in the analysis of IMCs and porous regions, both in terms

of calculated area [mm^2] and in terms of fractional area [%]. The data indicates a relationship between the increase in energy density and the expansion of IMCs area within the weld bead, as depicted in Fig. 5 and as shown in a previous study [7].

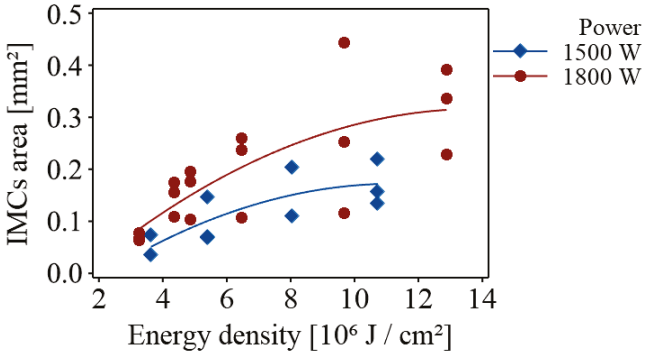

Fig. 5. Scatterplot of IMCs area vs Energy density.

This trend is mainly attributed to power. Higher power levels involve a more significant blending between copper and aluminum, which can promote the formation of IMCs. When welds with the same level of power output are compared, the separation distance becomes the most critical parameter for the same spiral diameter. This is because smaller separation distances, which also imply a greater overlapping, lead to an increased interface area and an enhanced element mixing. On the contrary, welding speed in the range tested does not significantly affects the characteristics of IMCs. The correlation between the weld bead and interface areas with the IMCs region is validated by the fractional area analysis. The results show that the fractional index for the IMCs area continuously stays at about 4-5% of the total bead area for all parameter sets. In Fig. 6, the scatterplot illustrates the relationship between porosity fraction and energy density. The formation of porosity is more significant at the lowest and highest energy densities. The separation distance is the parameter that has the greatest influence when it comes to welds carried out at low energy density. Separated spirals promote the occurrence of porosity in the melt-pool's stagnation areas, which are located at the interface on the aluminum side, micrograph (a) in Fig. 6.

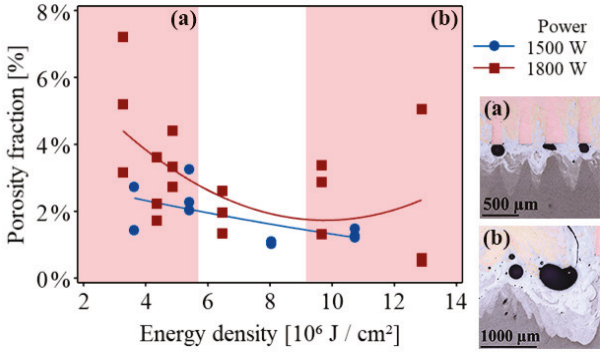

Fig. 6. Scatterplot of Porosity fraction vs Energy density with porosity typology.

As the separation distance decreased, a suppressive effect on stagnation porosity was observed, ultimately leading to a reduction in the porosity fraction. This trend reverses again when an excessively high energy density causes the melt-pool to become unstable.

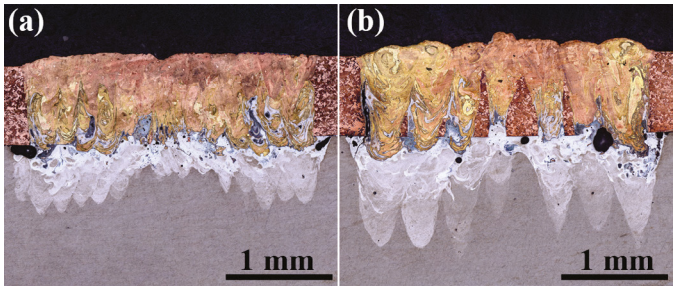

Fig 7: Optimised weald beads obtained with the following parameters: a) P=1500 W, v=150 mm/s, SD=0.2 mm and b) P=1800 W, v=150 mm/s, SD=0.4 mm.

The reason for the instability at high power is due to the intensified dynamics of the melt-pool, which causes excessive turbulence. Additionally, the keyhole phenomena at high energy densities oscillates between the complete opening and closing of the keyhole. As a result, at higher energy density, porosity formation restarts within the bead, as shown in Fig. 6 (b). Optimized welds were finally obtained for medium energy densities in the range of 8-10 MJ/cm^2, shown in Fig. 7.

4. Conclusion

An image algorithm was presented for the optimization of thick lap joint welds of Cu-Al dissimilar plates. The impact of laser parameters and scanning strategy was correlated to the primary defects occurring in these welds: intermetallic compounds and porosity. The results show an increase of IMCs with energy density, in particular for high power and low separation distance between the spirals. A decrease in the separation distance of the welding strategy is beneficial for IMCs due to the lower melted area and allows for reduced pore generation caused by melt-pool instability. However, the optimum parameters should avoid porosity formation in stagnation areas of the melt-pool. Finally, energy density between 8 and 10 MJ/cm^2 was defined as optimal.

References

[1] Sadeghian, A., Iqbal, N., 2022. A review on dissimilar laser welding of steel-copper, steel-aluminum, aluminum-copper, and steel-nickel for electric vehicle battery manufacturing. Opt. Laser Technol 146, 107595.
[2] B., Gao, X., Huang, Y., Gao, P.P., Zhang, Y., 2023. A review of laser welding for aluminium and copper dissimilar metals. Opt Laser Technol 167, 109721.
[3] Schmalen, P., Plapper, P., 2016. Evaluation of Laser Braze-welded Dissimilar Al-Cu Joints. Physics Procedia 83, 506–514
[4] Schmalen, P., Plapper, P., 2017. Resistance Measurement of Laser Welded Dissimilar Al/Cu Joints. JLMN 12.
[5] Braunovic, M., Alexandrov, N., 1994. Intermetallic compounds at aluminum-to-copper electrical interfaces: effect of temperature and electric current. IEEE Trans. Comp., Packag., Manufact. Technol. A 17, 78–85.
[6] Li, Q. et al. 2023. Effect of spiral scan distance on the nanosecond-pulsed-laser lap joint of Al/Cu. Opt Laser Technol 158, 108896. 6
[7] Pfeifer, S., Großmann, S., Freudenberger, R., Willing, H., Kappl, H., 2012. Characterization of Intermetallic Compounds in Al-Cu-Bimetallic Interfaces, in: 2012 IEEE 58th Holm Conference on Electrical Contacts (Holm), Portland, OR, USA, pp. 1–6.
[8] Ali, S., Shin, J., 2022. In-Depth Characterization of Laser-Welded Aluminum-and-Copper Dissimilar Joint for Electric Vehicle Battery Connections. Materials 15